ONCOLOGY

5-Azacytidine treatment inhibits the development of lung cancer models via epigenetic reprogramming and activation of cellular pathways with anti-tumor activity

Raluca Andrada Munteanu[1], Cristian Silviu Moldovan[1], Adrian Bogdan Tigu[1], Rares Drula[1], Richard Feder[1], Lorand Magdo[2], Ancuta Jurj[2], Lajos Raduly[2], Liviuta Budisan[2], Radu Pirlog[2], Alin Moldovan[1], Alina-Andreea Zimta[1], Cornelia Braicu[2], Alexandra Preda[3,4], Vlad Munteanu[5], Mihai Romitan[1], Diana Gulei[1], Tudor Eliade Ciuleanu[3,4]

1) MedFuture-Research Center for Advanced Medicine, Iuliu Hatieganu University of Medicine and Pharmacy, Cluj-Napoca Romania

2) Research Center for Functional Genomics, Biomedicine and Translational Medicine, Iuliu Hatieganu University of Medicine and Pharmacy, Cluj-Napoca, Romania

3) Department of Oncology, Iuliu Hatieganu University of Medicine and Pharmacy, Cluj-Napoca, Romania

4) Department of Oncology, Prof. Dr. Ion Chiricuta Oncology Institute, Cluj-Napoca, Romania

5) Department of Urology, Prof. Dr. Ion Chiricuta Oncology Institute, Cluj-Napoca, Romania

Abstract

Background and aims. Non-small cell lung cancer (NSCLC) treatment is challenged by late detection and limited therapeutic options. Aberrant DNA methylation, a common epigenetic alteration in NSCLC, offers new therapeutic avenues. This study aims to evaluate the combined effects of 5-Azacytidine (5-Aza), an epigenetic modifier, and ionizing radiation (IR) on NSCLC, exploring the underlying molecular mechanisms and therapeutic potential.

Methods. In this study, we examined the effects of 5-Aza combined with IR in both *in vitro* and *in vivo* models of NSCLC. Five human NSCLC cell lines were treated with 5-Aza and IR. Cell viability, colony formation, wound healing, and transwell migration assays were performed to assess treatment effects. Microarray and qPCR analyses were conducted to identify gene expression changes. Additionally, subcutaneous and orthotopic xenograft models were used to evaluate the treatment's efficacy *in vivo.*

Results. Treatment with 5-Aza and IR resulted in significant reductions in cell viability, colony formation, and migration in NSCLC cell lines. Microarray analysis revealed significant changes in gene expression, including the upregulation of apoptosis-related genes and the downregulation of cell proliferation-related genes. *In vivo* studies demonstrated a notable reduction in tumor growth and metastasis in both subcutaneous and orthotopic NSCLC models following 5-Aza and IR treatment. Histological and bioluminescent imaging confirmed the therapeutic effects of the combined treatment.

Conclusions. The combination of 5-Aza and IR shows promise as an effective treatment for NSCLC, enhancing apoptosis and reducing tumor growth through epigenetic modulation.

Keywords: NSCLC, epigenetic alterations, DNA methylation, cancer inhibitory effects, *in vivo* models

DOI: 10.15386/mpr-2777

Manuscript received: 31.07.2024
Accepted: 20.08.2024

Address for correspondence:
Diana Gulei
diana.c.gulei@gmail.com

Introduction

Lung cancer continues to be the leading cause of cancer-related mortality globally, with NSCLC accounting for approximately 85% of all cases [1,2]. This high mortality rate is largely due to the late stage at which lung cancer is often diagnosed, as well as the limited efficacy of conventional therapies in treating advanced-stage disease [3]. In response, the focus has shifted toward the development of novel treatment approaches, among which epigenetic therapies that showed promising clinical results in other malignant pathologies, especially from the hematological sector due to their potential to modulate gene expression without altering the DNA sequence [4,5].

DNA methylation, a critical epigenetic mechanism, plays a significant role in regulating gene expression [6]. Aberrant methylation patterns, particularly the hypermethylation of CpG islands in the promoter regions of tumor suppressor genes, are a hallmark of many cancers, including NSCLC [7]. 5-Aza, a cytidine nucleoside analog, has shown promise in inhibiting DNA methyltransferases (DNMTs), thus reversing these aberrant methylation patterns, and reactivating silenced tumor suppressor genes [8,9].

The potential for cancer therapy is promising given the reversible nature of epigenetic alterations. Inhibitors that specifically target DNMTs have demonstrated potential in the reactivation of silenced tumor suppressor genes and the suppression of cancer cell proliferation [10]. At present, several epigenetic agents are being utilized in clinical settings or are being evaluated in clinical trials for a range of malignancies [11]. The interaction among various epigenetic alterations implies that employing a combinational strategy including numerous epigenetic agents could potentially improve the effectiveness of therapeutic interventions (Figure 1) [12]. This is highlighted by our study findings, which identified significant pathways, including apoptosis and the JAK/STAT signaling pathway, as important mediators of NSCLC response to epigenetic therapy.

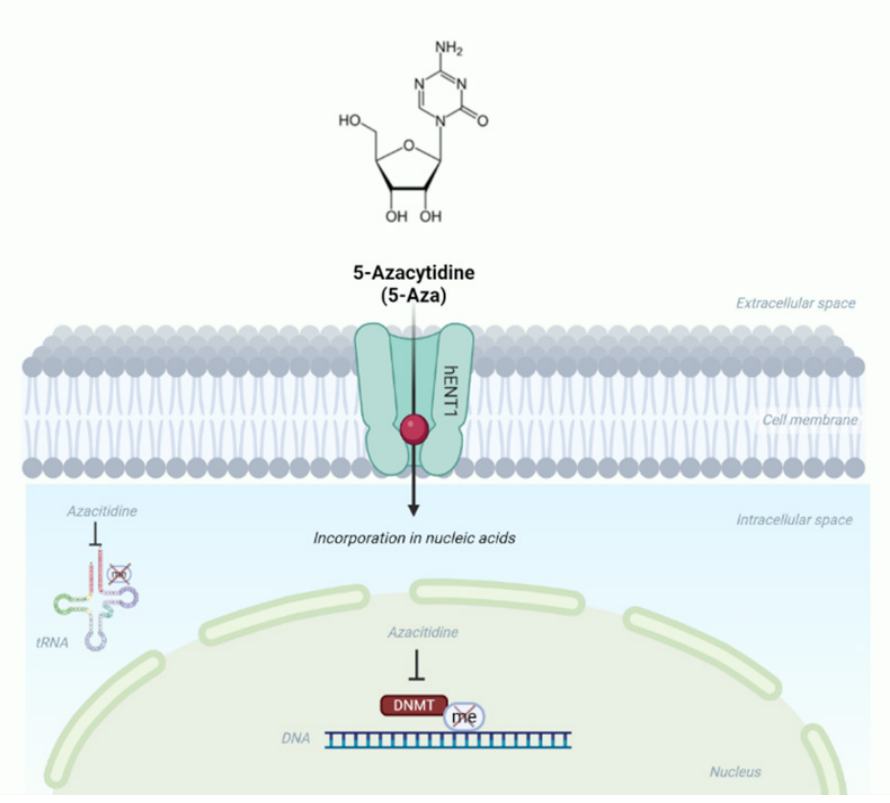

Figure 1. Mechanism of 5-Azacytidine Mediated Epigenetic Modulation in NSCLC Cells. 5-Aza is transported across the cell membrane and incorporated into nucleic acids. In the nucleus, it inhibits DNMTs, leading to DNA hypomethylation and subsequent reactivation of tumor suppressor genes. This process outlines the epigenetic modulation mechanism utilized by 5-Aza in the treatment of NSCLC.

5-Aza, primarily used for the treatment of myelodysplastic syndromes, has shown potential beyond hematologic malignancies, motivating research into its use for solid tumors like NSCLC [13]. The interest in combining 5-Aza with IR for NSCLC emerges from the urgent need for better therapies for this challenging disease, often diagnosed late with limited treatment options [14,15]. The ability of 5-Aza to demethylate DNA and reactivate dormant tumor suppressor genes may increase the sensitivity of cancer cells to DNA damage induced by IR and finally supporting the therapeutic combination of these treatments [16,17]. In preclinical models, this synergistic approach has improved cancer treatment efficacy, suggesting it could be more effective against NSCLC by utilizing their complementary mechanisms of action [18].

Our findings support this hypothesis, particularly through the validation of genes and pathways via microarray and PCR, clarifying their role in mediating the synergistic effects of combination therapy. Through evaluation using NSCLC cell lines and xenograft animal models, we aim to determine how 5-Aza and IR impact cell survival, apoptosis, and gene expression, and assess the feasibility of this approach as a potential treatment for NSCLC.

Methods

Cell lines and culture conditions

Five human NSCLC cell lines A549, A549-Luc2, SK-MES-1, H1792 and H522 were utilized in this study and were purchased from the American Type Culture Collection (ATCC). A549 and A549-Luc2 cell lines were cultivated in F-12K medium, fortified with 10% fetal bovine serum (FBS), while the H1792 and H522 cell lines were cultured in RPMI-1640 Medium, also supplemented with 10% FBS. SK-MES-1 cell line was cultured in medium with 10% FBS. All cell cultures were sustained at a stable condition of 37°C and 5%CO2.

Treatment regimens

In this study, we have designed two different regimens: a single dose of 5-Aza combined with 2 Gy of IR, and two doses of 5-Aza combined with 2 Gy of IR as represented in table I and II.

Table I. Single dose of 5-Aza combined with 2 Gy IR.

Experimental group	Treatment
Control Group	No therapeutic intervention
IR Group	Single dose of 2 Gy gamma radiation
5-Aza Group	Single administration of 5-Aza at the half-maximal inhibitory concentration (IC50)
5-Aza + IR Group	Single dose of 5-Azacytidine at the IC50, in conjunction with 2 Gy gamma radiation

Table II. Multiple-dose Protocol of 5-Aza (2X) combined with 2 Gy IR.

Experimental group	Treatment
Control Group	No therapeutic intervention
IR Group	Single dose of 2 Gy gamma radiation
5-Aza Group	Two sequential doses of 5-Aza at the IC50 concentration, with a 24-hour interval (without changing of culture medium)

Cell viability assay and determination of IC50 for 5-Aza

Cell viability assays were conducted to determine the half-maximal inhibitory concentration (IC50) of 5-Aza for A549, SK-MES-1, H1792 and H522cell lines. Cells were seeded at 1×10^4 cells per well in 96-well plates and treated 24 hours post-seeding with a gradient of 5-Aza concentrations ranging from 10nM to 5000nM. This gradient treatment was applied as a preliminary step to establish the IC50 for both treatment regimens.

Following a 48-hour incubation with 5-Aza, cell viability was assessed. The medium was removed, and cells were incubated with 150µl of thyazolyl blue tetrazolium bromide (1 mg/ml, Sigma, USA) for 1 hour at 37°C. Post-incubation, the tetrazolium dye was extracted, and cells were dissolved in 100µl DMSO. Absorbance was quantified using a TECAN SPARK10M plate reader (TECAN, Austria GmbH, Grodig). IC50 values were determined by nonlinear regression analysis using GraphPad Prism software.

Colony formation assay

Cells were collected from cultures via trypsinization and subsequently diluted to achieve a density of 500 cells per well. This cell suspension was evenly allocated in triplicate across a 6-well plate. For a period of three weeks, the plate was maintained under identical conditions as those used for routine culture. Following this incubation period, colony fixation was carried out using 80% methanol (MeOH), and staining was performed using a 0.5% solution of crystal violet. The quantification of colonies was accomplished through image analysis with ImageJ software.

Scratch assay

Cells were cultured in a 24-well plate until they reached confluence. A scratch was created in the cell monolayer of each well using a sterile pipette tip to remove cells in a straight line. Following a 24-hour adhesion period, the cells were washed with phosphate-buffered saline (PBS) to remove debris and then incubated with fresh, serum-free medium to inhibit cell proliferation and focus on migration. Images of the scratch area were taken at regular intervals until the gap was closed in at least one experimental condition, with all images captured at 100x magnification. The gap area was then measured using ImageJ software.

Transwell

A549 cells were first prepared in serum-free medium and then transferred to the top compartment of Transwell inserts, which feature a polycarbonate membrane. These inserts, supplied by Corning (New York, United States), had been pre-coated with a 5% solution of Geltrex, courtesy of Thermo Fisher Scientific (Waltham, MA, USA). The assay's bottom compartment was filled with a complete medium enriched with FBS. This setup was incubated for 24 hours to facilitate cell migration through the membrane. Following incubation, the inserts were fixed using 4% paraformaldehyde (PFA) and subsequently stained with a 0.1% crystal violet solution. To quantify migration, images from three randomly selected fields were taken and analyzed. The extent of area covered by migrated cells was assessed using Image J software.

Confocal microscopy

Cells were cultured in chamber slides using their respective media under the experimental conditions previously described. Permeabilization was performed with 0.5% Triton X-100, followed by staining of the mitochondria using the Mitochondrial Staining Kit – Red Fluorescence (Abcam, Cambridge, UK) for 1 hour in fresh PBS at 37°C with 5% CO_2. After staining, cells were washed three times with PBS.

For fixation, cells were treated with 4% paraformaldehyde (PFA) for 10 minutes at room temperature. Actin filaments were then stained with Phalloidin-FITC (Acti-stain™ 488 Fluorescent Phalloidin, Cytoskeleton Inc, Denver, USA) for 30 minutes at room temperature, followed by three washes with PBS. Nuclei were stained with DAPI (Abcam, Cambridge, UK) at a concentration of 100 µg/mL for 30 seconds, followed by three additional washes with PBS. The chamber slides were mounted using ProLong Gold Antifade Mountant.

Imaging was conducted using an Olympus FLUOVIEW FV1200 laser scanning fluorescence confocal microscope, equipped with a PLAPON60xOSC2 (1.4 NA) objective. Images were acquired in sequential mode across three channels with excitation at 405 nm, 488 nm, and 543 nm. The specific settings for image acquisition were adjusted based on the fluorescent dyes using the FV10-ASW 4.2 software. Post-acquisition image processing was performed using ImageJ.

Fluorescence microscopy

Cells grown in chamber slides were permeabilized using 0.5% Triton X and stained with CytoPainter Mitochondrial Staining Kit – Red Fluorescence (Abcam, Cambridge, UK) for one hour, in fresh PBS, at 37°C, under 5% CO2. Thereafter cells were washed three times in PBS buffer and fixed in 4% (w/v) paraformaldehyde for 10 min at room temperature. Phalloidin-FITC (ActistainTM 488 Fluorescent Phalloidin, Cytoskeleton Inc, Denver, USA) was then added and incubated at room temperature for 30 min, in darkness. The cells were washed three times with PBS and then the nuclei were stained with DAPI (Abcam, Cambridge, UK) 100 µg/mL for 30 seconds, followed by another step of washing with PBS. The chamber slides were mounted in ProLong Gold Antifade Mountant. Dark-field microscopy was performed using an Olympus B × 43 microscope (Olympus, Tokyo, Japan) equipped with a CytoViva Enhanced Dark-Field Condenser (Cytoviva, USA), a Dual Mode Fluorescence (DMF) module, an UPlanFLN60×, NA = 1.2 oil immer-sion objective (Olympus, Tokyo, Japan) and a 6.4 µm/pixel CCD camera (QImaging, Can-ada). Images were calibrated for scale and annotated in ImageJ2.0.

Flow cytometry for apoptosis evaluation

For apoptosis evaluation, treated and control A549 cells were rinsed with binding buffer, stained with Annexin-V FITC and incubated 10 minutes on ice. After incubation, cells were centrifuged for 5 minutes at 2000 x g and resuspended in 250µl binding buffer. Before acquisition, PI (propidium iodide) was added, and the cell death events were analyzed using a BD FACSCanto II flow cytometer; obtained data was processed with FACS Diva version 6.0 software.

Microarray analysis

Total RNA extraction was executed using TriReagent (Thermo Fisher), followed by purification using the RNeasy Mini kit (Qiagen) according to the manufacturer's protocol. Subsequently, the RNA concentration was quantified utilizing a Nanodrop-ND-2000 spectrophotometer, and RNA quality was assessed through Bioanalyzer 2100 (Agilent Technologies). Samples achieving an RNA Integrity Number (RIN) exceeding 7 were considered as meeting the necessary standards for further analyses.

The gene expression evaluation was done starting from 200 ng of total RNA using Agilent one colour microarray protocol and Low Input Quick Amp Labeling Kit. Prior to hybridizatiion, the microarray probes (cRNA-Cy3) underwent purification using the RNeasy Mini Kit (Qiagen, Germany). All the microarray probes designated for hybridization demonstrated a minimum of 1.65 µg and a specific activity exceeding 6 pmol/µL Cy3.

Hybridization was carried out for 17 hours at 65°C using 8 × 60 k v2 microarray slides (G4851B) according with the manufacturer's protocol. Subsequently, the microarray slides were scanned using an Agilent G2565CA microarray scanner.

Following the microarray slide scanning process, image data was processed and numerical values for gene expression were extracted using the Feature Extraction software (Agilent Technologies). Data normalization was executed using the GeneSpring GX program (Agilent Technologies), applying the quantile algorithm.

To enhance data quality, control probes were excluded, and entities were filtered based on flag values, retaining those classified as 'detected' while discarding others. Differentially expressed transcripts were identified using the 'Filter on Volcano Plot' module with moderated t-test, imposing a fold change threshold of 2.0 and a p-value < 0.05 for each treatment scheme relative to its respective control. Furthermore, to minimize the occurrence of false positives, we implemented the Benjamini-Hochberg procedure, a well-established method for controlling the false discovery rate (FDR). The resulting datasets were exported to Excel (Microsoft) for subsequent analysis.

Sample processing for RNA extraction

Total RNA was extracted from cultured A549 cells post-treatment. Cells were harvested, washed with PBS, and lysed with 800 µL of TripleXtractor reagent (Grisp, Portu-gal). The lysates were stored at -80°C after snap-freezing in liquid nitrogen.

For RNA purification, samples were thawed and mixed with 160 µL of chloroform, then centrifuged to separate the phases. The aqueous phase was transferred to a new tube, to which isopropanol was added for RNA precipitation. After a second centrifugation, the RNA pellet was washed with 75% ethanol, air-dried, and rehydrated in ultrapure water. RNA concentration and quality were assessed using a NanoDrop 3000 spectrophotometer (Thermo Scientific, Waltham,USA).

DNAse treatment protocol

Total RNA samples were treated with DNAse to remove any potential genomic DNA contamination. To each 10 µL RNA sample, 1.75 µL of TURBO DNA-free mix was added, following the composition outlined in the table below. The mixture was incubated for 30 minutes at 37°C in an Applied Biosystems Veriti 96-well thermal cycler. Post-incubation, 2 µL of DNase inhibitor was added to neutralize the DNase activity, and samples were vortexed, incubated at room temperature for 5 minutes, and centrifuged at 17,000 x g for 2 minutes. The supernatant, containing the purified RNA, was then transferred to a new tube.

RNA concentration was subsequently quantified using the NanoDrop 3000 spectrophotometer to ensure adequate purity and concentration for downstream applications.

cDNA synthesis

Before starting the cDNA synthesis, all RNA samples were diluted to reach 500 ng/uL of pure treated RNA (as previously described). For cDNA synthesis we used High-capacity cDNA Reverse Transcription Kit (Applied biosystems, USA). And 10 uL of RNA were mixed with 10 uL of master mix. The mix was performed in sterile 200 uL Eppendorf tubes and the reaction ran using the predefined program using Applied biosystems Veriti 96 well thermal cycler. 10 minutes at 25°C, followed by 2h of incubation at 37°C, then 5 minutes at 85°C and then the samples were kept on ice or stored at -20°C. The resulted mix contains the cDNA corresponding to the 5000 ng of total RNA included in the reaction. The cDNA was diluted 1:5 and then further used for the RT PCR analysis for gene expression.

RT-PCR

RT-PCR was performed in 96 well plates compatible with the STEPONEPLUS RT PCR instrument (Applied Biosystems, USA) using SyBr green mastermix, at a final vol-ume of 20 uL/reaction. 19 uL of each master mix were loaded in the 96 well plates and 1 uL of cDNA was added directly in the plated in the corresponding place on the plate. The RT-PCR analysis used the following amplification program from table III. After cycling, the Melting curve analysis was performed for every single analysis.

Table III. RT-PCR amplification program.

50ºC	2 minutes	Hold
95ºC	2 minutes	Hold
95ºC	3 seconds	40 cycles
60ºC	30 seconds	40 cycles

Animal strains and husbandry

Pathogen-free eight-week-old female immunodeficient athymic nude mice (n=10) purchased from (Charles River, Hungary) were included in the study. Following transportation to the vivarium, a quarantine and acclimation period of one week was implemented. The murine subjects were housed in a pathogen-free environment utilizing an IVC2-SM-56-IIL rack system (Acellabor, HU), featuring individually ventilated cages that employed Hepa-filtered air (II L Cages). Unrestricted access to autoclaved water and pelleted nourishment was facilitated. Additionally, bedding material, from Lignocel (Rosenberg, Germany), was subjected to autoclaving in compliance with standardized protocols. Habitat conditions at the Research Center for Advanced Medicine, Medfuture, Iuliu Hatieganu University of Medicine and Pharmacy were controlled, with a thermal range maintained at 22°C ± 2°C, relative humidity at 55% ± 10%, and under a diurnal cycle comprising 12-hour light and dark intervals. Experimental protocols were executed following ethical approval from the Ethics Committee of Iuliu Hatieganu University of Medicine and Pharmacy (Approval No. 47/12.03.2024) and in strict compliance with EU Directive 63/2010. After the acclimation phase and prior to experimental engagement, the subjects were marked with metallic auricular tags and isolated from the general murine population.

Subcutaneous xenograft mouse model

The mice were (n=8) subcutaneously injected in the right flank with $2x10^6$ A549 cells, following treatment according to "Treatment Scheme 2". The animals were divided into four experimental cohorts, each containing two mice, based on the *in vitro* treatment received as follows:

a. Control Group: No treatment administered.

b. IR Group: Exposure to 2 Gy of gamma radiation

c 5-Aza Group: Treatment with two doses of 5-Aza, utilizing an IC50 concentration.

d. 5-Aza + IR Group: Treatment with two 5-Aza doses (IC50 concentration) and exposure to 2 Gy of gamma radiation.

For a period of 30 days, the development of the subcutaneous xenografts was monitored through bi-weekly measurements of tumor diameters. In addition, biometric assessments of the tumors and weighing of the animals were executed once every three days for the entire study period.

Upon reaching the 32-day mark, the animals were euthanized in compliance with standard guidelines, and the tumors were excised, measured, and weighed. After undergoing macroscopic analysis, the tumor tissue was submitted for histological examination.

Orthotopic xenograft mouse model

Orthotopic xenograft models (n=2) were established utilizing $2x10^6$ A549-Luc2 cells injected into murine right lung tissue via open survival surgery. Prior to the procedure, analgesia was ensured with slow-release buprenorphine (1.0 mg/kg), while anesthesia was induced and maintained at 2.5% and 2% isoflurane, respectively. Anatomically injections involved a 1–1.5 cm incision at the middle axillary line, expedited through a right lateral decubitus position dependent upon the lung target. Following tissue and fascia dissection, cells were orthotopically injected, employing an intra-parenchymal approach at the third intercostal space, with subsequent suture and monitored recovery on heating pads.

Longitudinal *in vivo* monitoring of xenograft development was executed using the IVIS SPECTRUM (Perkin Elmer, USA), using a bioluminescent reporter (IVISbrite D-luciferin, RediJect, Perkin Elmer). Following model establishment on day 12, mice were divided into control and treatment cohorts, receiving bi-weekly intraperitoneal doses of 5-Azacytidine (5 mg/kg in 150 µl saline) over two weeks. Efficacy monitoring was achieved using recurrent IVIS Imaging, concluding in terminal macroscopic metastatic analysis post-euthanasia after 32 days.

Tumor growth and animal follow-ups

The animals underwent systematic imaging sessions with a bi-weekly frequency following implantation. Concurrently, we documented the animals' body weights and conducted assessments of their overall wellbeing. This included the identification of signs of distress and the surveillance of symptoms associated with NSCLC lung tumors, including dyspnea, rapid weight loss, as well as conventional markers of murine distress, such as asthenia, lethargy, reduced grip strength, decreased locomotor activity, and impaired grooming. Continuous monitoring was sustained for a duration of 30 days in the subcutaneous group and 32 days in the orthotopic group.

Bioluminescent imaging (BLI)

In vivo tumor progression was monitored through bioluminescence imaging (BLI) employing the Caliper IVIS Imager (PerkinElmer) and analyzed using Living Image 3.2 software. Imaging sessions were conducted with exposure durations ranging from 1 to 300 seconds and binning settings varying from 2 to 8.

To initiate imaging, mice from the orthotopic cohort received an intraperitoneal injection of 150 mg/kg D-luciferin in PBS. Images were acquired after 10 minutes post-injection, with mice maintained under isoflurane anesthesia. The total photon flux, quantified in photons per second, was determined within regions of interest (ROIs) covering the entire dorsal and ventral aspects of each mouse. The optical signal was subsequently normalized to the average radiance, expressed in photons per second per square centimeter per steradian (p/s/cm2/sr).

H&E staining

The lung samples were fixed for two days using a 4% paraformaldehyde solution (Servicebio). After dehydration and embedding processes, the samples were sliced into slices with a thickness of 5 µm. Subsequently, an H&E staining kit (Beyotime) was used for the experimental procedure. Prior to staining with hematoxylin for a duration of 5 minutes, the lung sections were subjected to a deparaffinization and rehydration procedure. Following a rinsing procedure, the sections were subjected to differentiation for a duration of 30 seconds. Subsequently, the specimens were subjected to a washing process followed by a one minute treatment with eosin. Following a series of sequential rinsing, dehydration, and permeabilization procedures, the sections were subsequently sealed with neutral resin. Finally, the sections were subjected to microscopic analysis at a magnification of 100x.

Results

Response of NSCLC cell lines to increasing doses of 5-Aza

To investigate the effect of 5-Aza on lung cancer we treated four lung cancer cell line models with increasing doses of 5-Aza. After 48 hours of treatment, the A549, SK-MES-1, H1792 and H522 cell lines exhibited IC50 values of 2218 nM, 1629 nM, 1471 nM and 1948 nM, respectively. Despite not having the lowest IC50 value, the A549 cell line indicated a dose-dependent decrease in cell viability with increasing concentrations of 5-Aza and was further used for functional studies (Figure 2). A separate study should be employed to elucidate the differences in dose and time response between the lung cancer cell lines, considering that, in theory, all the four cell lines exhibit aberrant methylation patterns with cancer development roles.

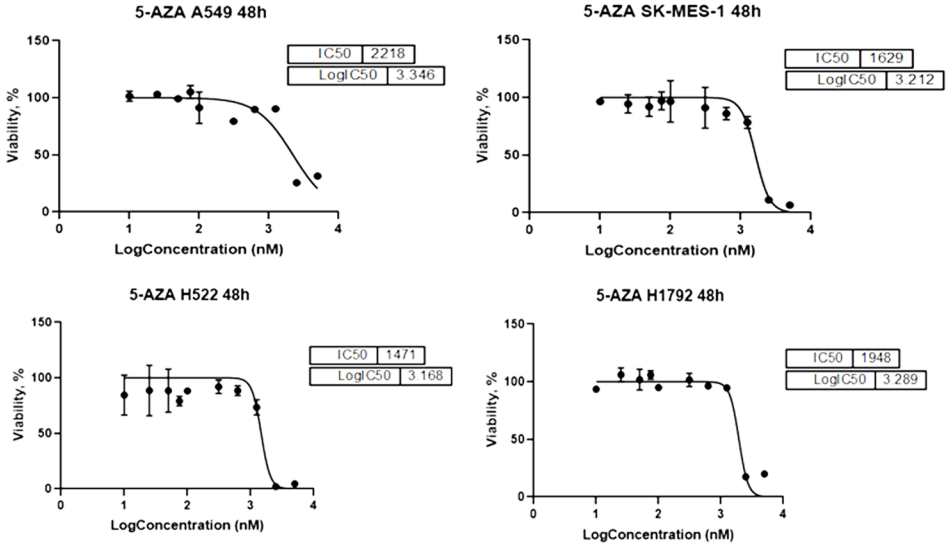

Figure 2. IC50 Values of NSCLC Cell Lines to 5-Aza Treatment. The graph shows dose-response curves for A549, SK-MES-1, H522, and H1792 cell lines after 48-hour treatment with 5-AZA, demonstrating varying drug sensitivities.

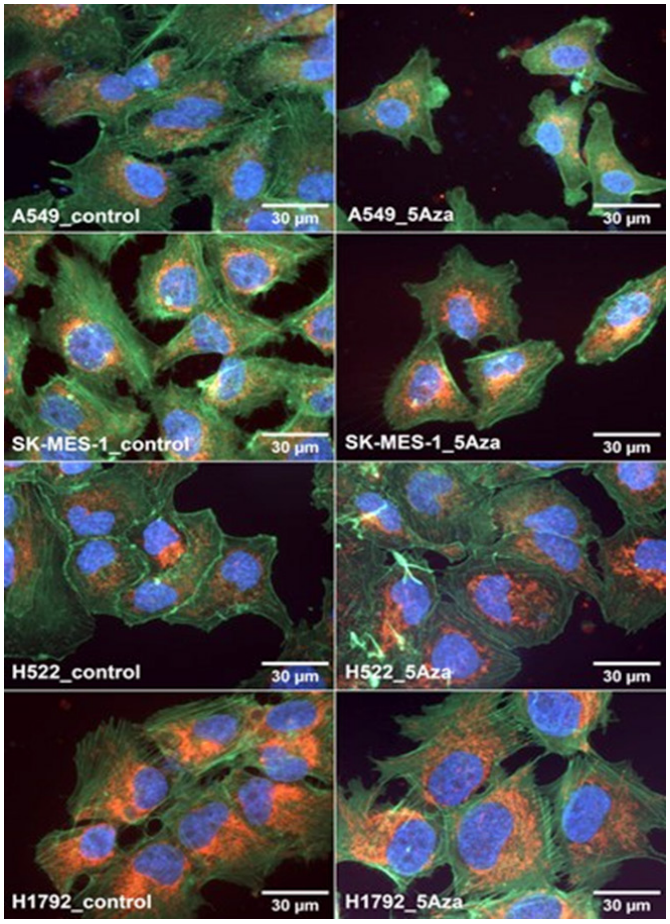

Figure 3. Fluorescence microscopy images of different untreated cells (left panel) and treated with 5-Aza (right panel) lung cancer cell lines. Red fluorescence indicates viable mitochondria, blue fluorescence shows nuclei and green fluorescence shows actin filaments (cytoskeleton).

Morphological and functional alterations in lung cancer cell lines post 5-AZA treatment

The dark field fluorescence microscopy shows four different lung cancer cell lines: A549, SK-MES-1, H522, and H1792 imaged as controls and with their corresponding 5-Aza treated samples at 48 hours. The control samples displayed cells with well-organized cytoskeletons, as suggested by the FITC-labeled actin filaments. Moreover, untreated cells maintained their round or oval shaped nuclei (stained blue), while the red staining highlighted the presence of active mitochondria (Figure 3).

Following the 5-Aza treatment, the cells exhibit noticeable alterations in their morphology. All cell lines showed cytoskeletal disruption, including filament fragmentation and disorganization. These changes suggest structural damage to the cytoskeleton. Compared to control cells, treated cells had irregular shapes and less contact between them, indicating altered cellular arrangement.

The nuclear morphology in the cells treated with 5-Aza shows modifications, with certain nuclei having a more condensed or irregular outline. These changes are often associated with stress responses or apoptotic processes.

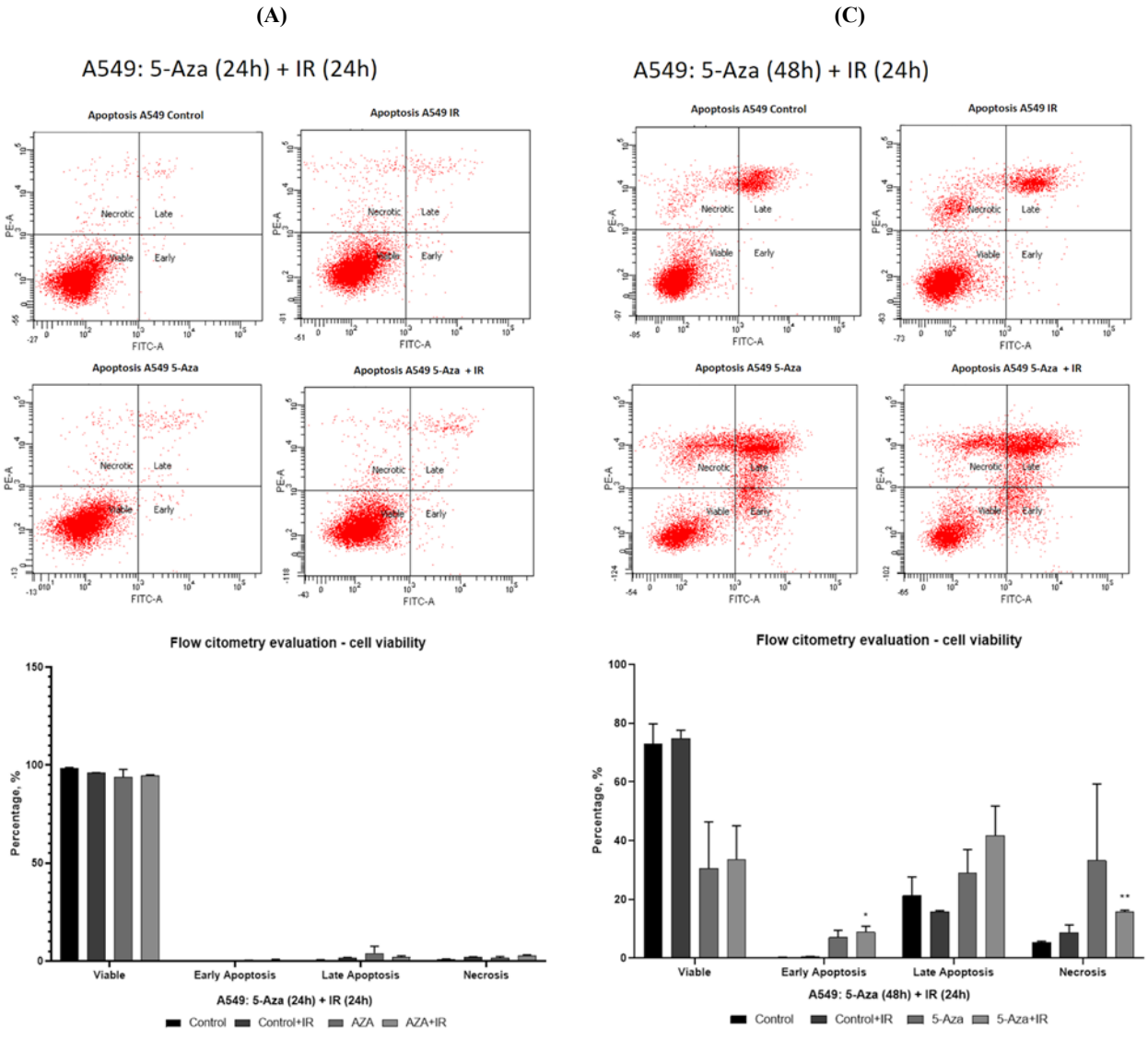

Figure 4. Flow Cytometric Analysis of A549 Cell Viability Under Combined 5-Azacytidine and Ionizing Radiation (IR) Treatment Protocol. Panel A presents flow cytometry analyses of A549 cells subjected to 24-hour treatments of control, IR, 5-Aza, and 5-Aza with 2 Gy of IR. AnnexinV staining quantification is correlated to cell mortality (early and late apoptosis stages), while PI staining indicates late apoptosis and necrosis. Graphical representations of the different types of cell death induced by 5-Aza/5-Aza+ 2 Gy of IR at 24h and 48h are illustrated in Panels B and D, respectively.

The fluorescence intensity of the mitochondrial dye decreased in the treated cells, indicating either a reduction in mitochondrial function or a decrease in the number of metabolically active cells following treatment. As illustrated in figure 3, the A549 cell line demonstrated the most significant reduction in mitochondrial staining after treatment. This observation suggests a decrease in metabolic function and disruptions in actin structure, indicative of structural changes within the cells. Additionally, alterations in nuclear morphology were observed, consistent with potential cell cycle arrest or the initiation of apoptosis. These cellular processes were further evaluated using additional biochemical assays using A549 as a model cell line for the study.

5-Aza and IR synergistically affect cell viability in A549 cell line

To investigate the combined effect of 5-Aza and IR on the A549 cell line, we performed a series of flow cytometry assays to measure cell viability. The assays revealed that treatment with 5-Aza alone for 24 hours had a minimal impact on inducing cell death. However, extending the treatment to 48 hours significantly increased the cell death rate. Additionally, combining 5-Aza with IR further enhanced the reduction in cell viability.

The flow cytometry results, illustrated in figure 4, in panels A and C, show the proportion of apoptotic cells following treatment with 5-Aza for 24 and 48 hours, both with and without concurrent IR. The data indicate an increase in the apoptotic population at the 48-hour time point, especially when 5-Aza is combined with 2 Gy of IR. Quantitative analysis of these results, presented in panels B and D, confirm the increase in both early apoptosis and late stages of necrosis, suggesting that the combined treatment has a greater effect on reducing cell viability than either treatment alone. The data supports the hypothesis that 5-Aza demethylating activity, in conjunction with the DNA damage induced by IR, leads to a synergistic effect, resulting in an increased apoptotic response in the A549 lung cancer cell model.

The minimal differences at 24 hours post-treatment with agents like 5-Aza could be due to the time required for drug action to manifest, especially when it alters gene expression through changes in DNA methylation.

However, the biological processes influenced by 5-Aza, such as DNA methylation, transcriptional activation, and interference with the cell cycle, might take more than 24 hours to affect the cell population. Moreover, the cells need time to progress through the cell cycle for 5-Aza to be incorporated into the newly synthesized DNA and for subsequent rounds of cell division to be affected.IR, on the other hand, causes immediate damage to the DNA, but the cellular response, which includes DNA repair, cell cycle arrest, and eventually apoptosis if the damage is irreparable, may also take time to be observed.

By 48 hours, more cells have likely accumulated sufficient damage or have had enough time to undergo the biochemical changes leading to the observed phenotypes of cell death.

Morphological evidence of cellular stress in 5-Aza and IR treated A549 cells

Figure 5 shows microscopy images of the A549 cell line, depicted both in bright-field (top row) and confocal microscopy (bottom row), under four different conditions: control, IR, 5-Aza, and a combination of two doses of 5-Aza plus 2 Gy of IR treatment.

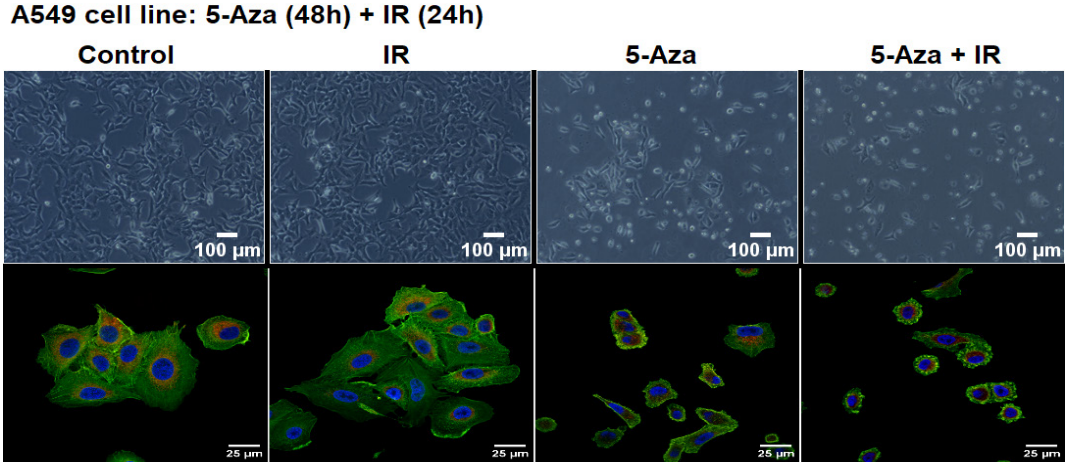

Figure 5. Bright-field images of A549 cells under various experimental conditions are depicted, including control, IR (irradiation), 5-Aza (5-Azacytidine treatment), and 5-Aza + IR (combined 5-Aza treatment and irradiation). In the bottom row are represented confocal microscopy images of the same conditions, which are triple stained to visualize different cellular components: actin filaments (green), nuclei (blue), and viable mitochondria (red).

In the bright-field microscopy, the untreated control cells showed typical confluent growth, with cells displaying elongated shapes and being equally distributed across the field. Following 2 Gy IR treatment, the cells maintain their confluency to some extent but appear slightly more dispersed, indicating a potential decrease in cell survival. The administration of 5-Aza as a standalone treatment results in a significant decrease in confluence, accompanied by an increase in intercellular space, indicating cell detachment and death. The combined administration of 5-Aza with IR enhanced this effect, resulting in a more pronounced spacing between cells and reduced confluency.

The confocal microscope images, on the other hand, offer a more detailed examination of the cells, displaying actin filaments labeled in green, nuclei stained with DAPI in blue, and viable mitochondria stained in red. The control cells presented well defined actin filaments, indicating a strong and organized cytoskeletal structure, spherical and uniformly stained nuclei, and a homogeneous distribution of active mitochondria. Following 2 Gy IR treatment, there were noticeable alterations in the arrangement of actin filaments, and the mitochondrial staining appeared slightly less homogenous. Cells treated with 5-Aza exhibited major morphological differences, characterized by disorganized actin filaments, irregularly shaped nuclei, and more scattered mitochondrial staining, indicating disrupted metabolic activity.

These features are particularly noticeable in the treatment that combines 5-Aza with IR. The cells showed fractured actin filaments, characterized by a sparse and disorganized appearance. Additionally, there is a decreased cell count in the field, most likely attributed to cell death. The nuclei are also irregular and varied in size, a common feature of apoptosis.

Although the membranes themselves are not specifically marked, we can assume the existence of membrane blebs in the confocal microscopy image of cells that have been exposed to both 5-Aza and IR, based on the labeling of actin filaments. This is shown by the presence of rounded, balloon-like projections that protrude from the cells, aligning with the regions where the actin cortex is damaged or missing.

The images illustrate the structural deterioration of A549 cells following treatment with 5-Aza and IR, supporting the results from flow cytometry and highlighting the potentiation of cellular stress and death indicators with the combined treatment.

5-Aza and IR synergistically affect the aggressive phenotype of A549 cell line

Colony formation assays were performed on A549 Luc cell line treated with 5-Aza and IR, both individually and in combination. This assay was performed on the A549 Luc cell line, selected for its relevance to imagistic evaluation of the *in vivo* models.

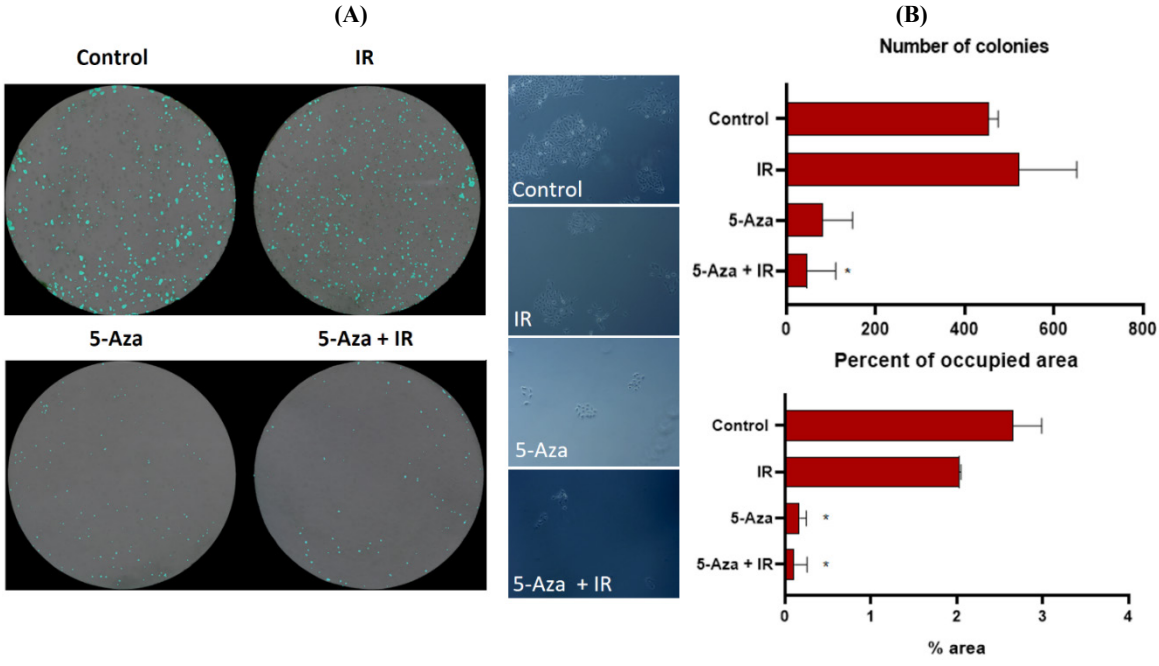

Figure 6. Effect of 5-Aza and IR on A549 Cell Colony Growth. Pannel A displays the clonogenic survival of A549 Luc cells under different treatment conditions, showing colony formation post treatment with 5-Aza, IR, and their combination. Pannel B quantifies these effects in terms of number of colonies (up) and percent of occupied area (down) for all the experimental models included in the study.

Treatment with IR and 5-Aza independently reduced colony formation compared to the untreated control. The combination of 5-Aza and IR resulted in a more pronounced decrease in both the number and size of colonies. Quantitative analysis showed a significant reduction in the number of colonies in the combined treatment group compared to all other groups. The percentage of occupied area by colonies further confirmed the substantial inhibitory effect of the combined treatment, as evidenced by a marked decrease in area occupied by colonies in the 5-Aza + IR group compared to the control, IR only, and 5-Aza only groups (Figure 6).

The wound healing assay was conducted to evaluate the migration of A549 cells under different treatment conditions: Ctrl, IR, 5-Aza, and a combination of 5-Aza + IR. The results are depicted in (Figure 7). In the control group, cells exhibited normal migration and wound closure, with the gap nearly closing by 80 hours. Both IR and Aza treatments demonstrated a moderate reduction in cell migration compared to the control. Notably, the combination of 5-Aza + IR resulted in the slowest wound closure, maintaining a higher percentage of the occupied area throughout the experiment. This indicates a pronounced synergistic inhibition of cell migration, suggesting that combining 5-Aza+IR is more effectively impedes cell migration and wound healing than either treatment alone.

Transwell assay confirms the reducing effect of 5-Aza upon the invasiveness of A549 cell line compared with control. While irradiation by itself does not possess a significant effect upon cell migration, 5-Aza combined with 2 Gy of IR impairs significantly the migration capacity of the cancerous pulmonary cells (Figure 8). The top left panel denotes the untreated control group, reflecting the baseline invasive behavior of the cells. The top right panel assesses the impact of IR alone, showing the cellular response to this single treatment variable. In the bottom left panel, cells treated with 5-Aza exhibit reduced migration, indicative of decreased invasiveness. The bottom right panel, displaying the combined treatment of 5-Aza and IR, demonstrates an amplified reduction in cell migration, suggesting a synergistic interaction between the two treatments in inhibiting cell invasiveness. This observation points to a synergistic effect of the combined treatments in further reducing the invasive potential of A549 cells. The variation in staining intensity reflects the relative quantity of cells that have migrated, with darker areas denoting higher densities of cells.

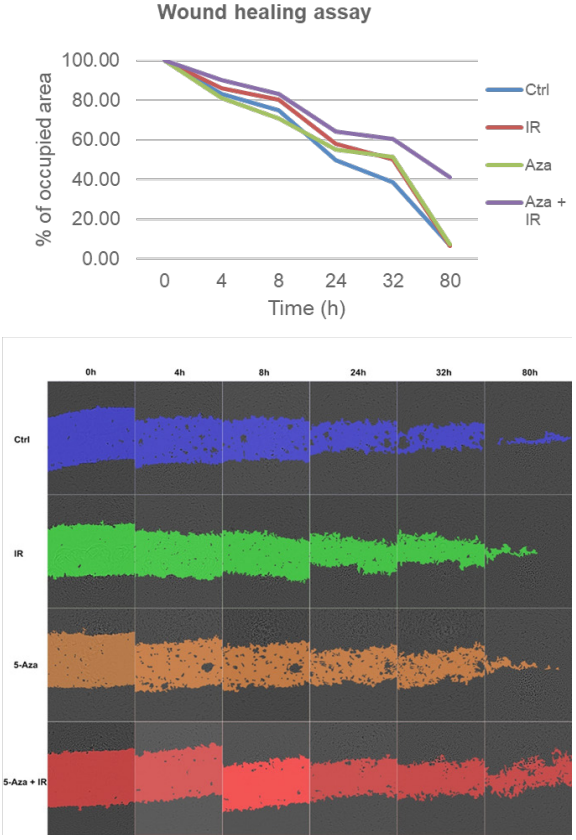

Figure 7. Upper Panel: Percentage of occupied area in a wound healing assay of A549 cells under different treatment conditions over time. Lower Panel: Graphical representation of wound closure.

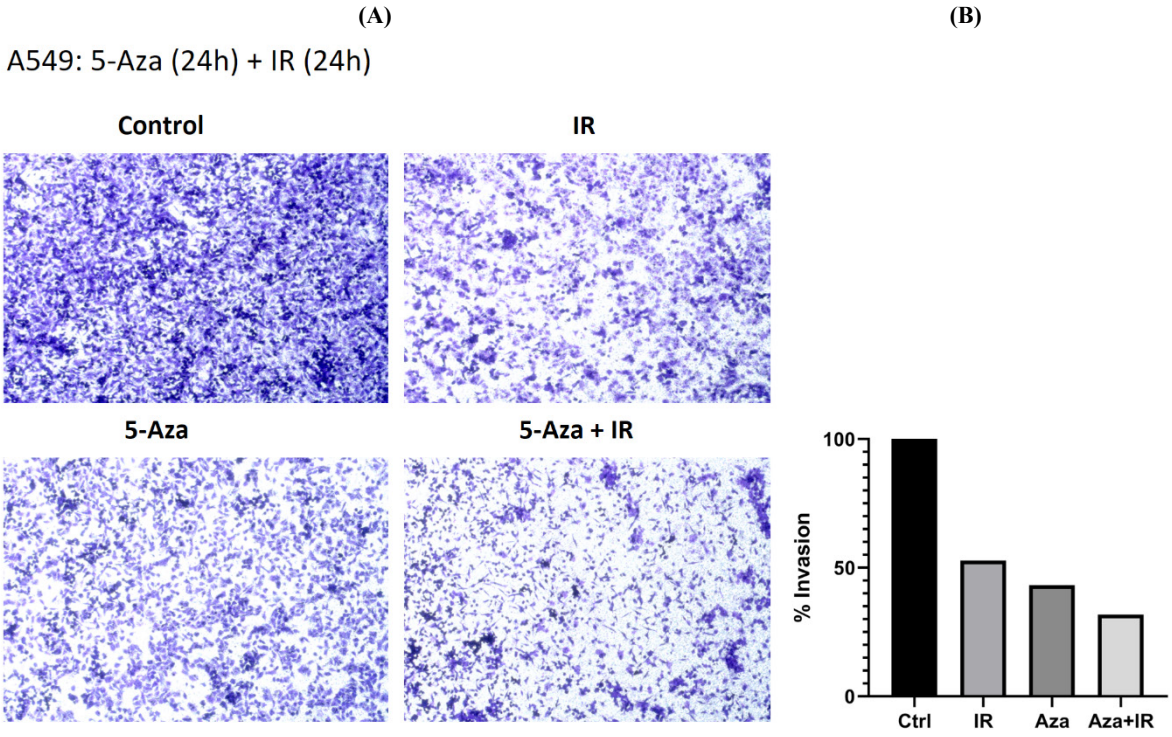

Figure 8. Transwell Migration Assay of A549 Lung Carcinoma Cells after 24 hours of treatment with 5-Aza and IR (24 hours post-treatment) (Left Panel). Quantification of the migrated A549 cells was performed by analyzing the area covered by cells in the images using ImageJ software. The results are presented as a bar graph showing the percentage of cell migration relative to the control group (Right Panel).

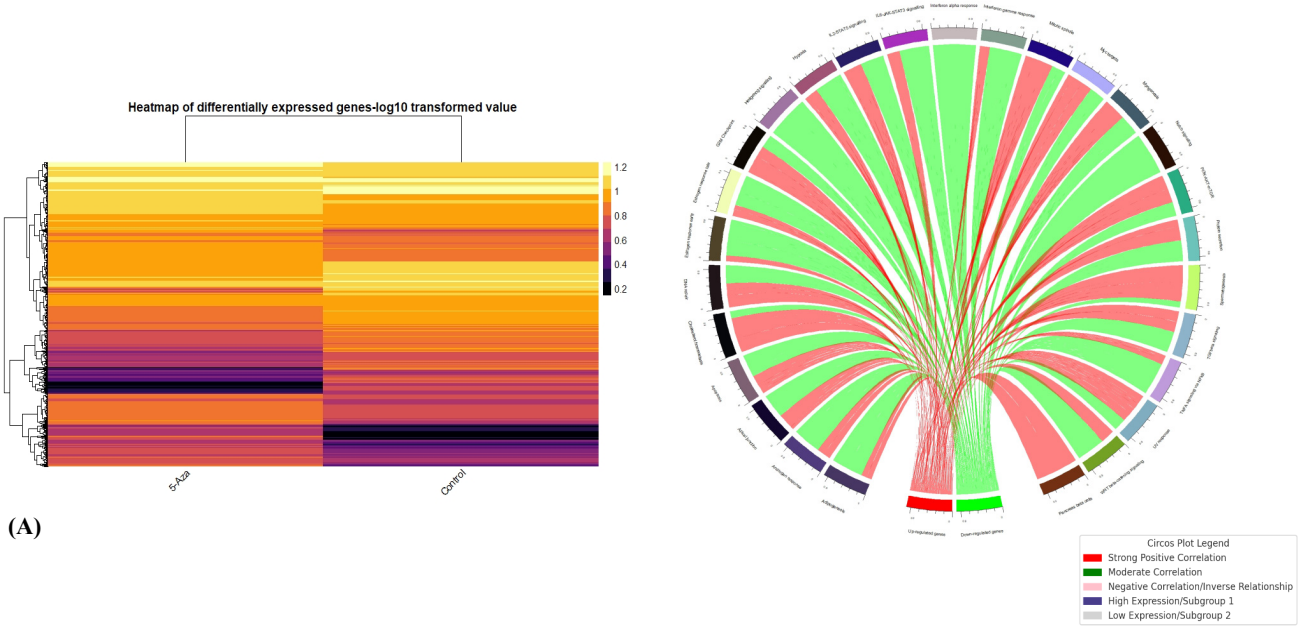

Figure 9. Heatmap and Circos Plot of Differentially Expressed Genes in A549 Cells Post-5-Azacytidine Treatment. Panel A shows a heatmap with log10 transformed expression values of genes altered by 5-Azacytidine treatment (orange indicates upregulation and purple indicates downregulation). Panel B presents a Circos plot showing the intergenic expression correlations post-treatment, the line thickness represents the strength of the correlation.

Differential gene expression in A549 cells following 5-azacytidine treatment

Microarray analysis highlighted an extensive spectrum of gene expression alterations following 5-Aza treatment in A549 cells (Figure 9). Across 10,013 genes, there was a significant shift in expression (average p-value = 0.0029), indicating a potent cellular response. We observed that 5,209 genes were upregulated, many of which are implicated in stress responses and apoptotic pathways, whereas 4,804 genes were downregulated, often associated with cell proliferation.

Enrichment analysis shows in figure 10 (Panel A) an enrichment score (ES) curve that demonstrates the overrepresentation of apoptosis-related genes at the top of the ranked list. Figure 10 (Panel B) illustrates an enrichment plot for the hallmark of JAK/STAT signaling gene set. Similar to the apoptosis plot, it presents the cumulative ES curve, with the peak suggesting a significant overrepresentation of JAK/STAT signaling genes.

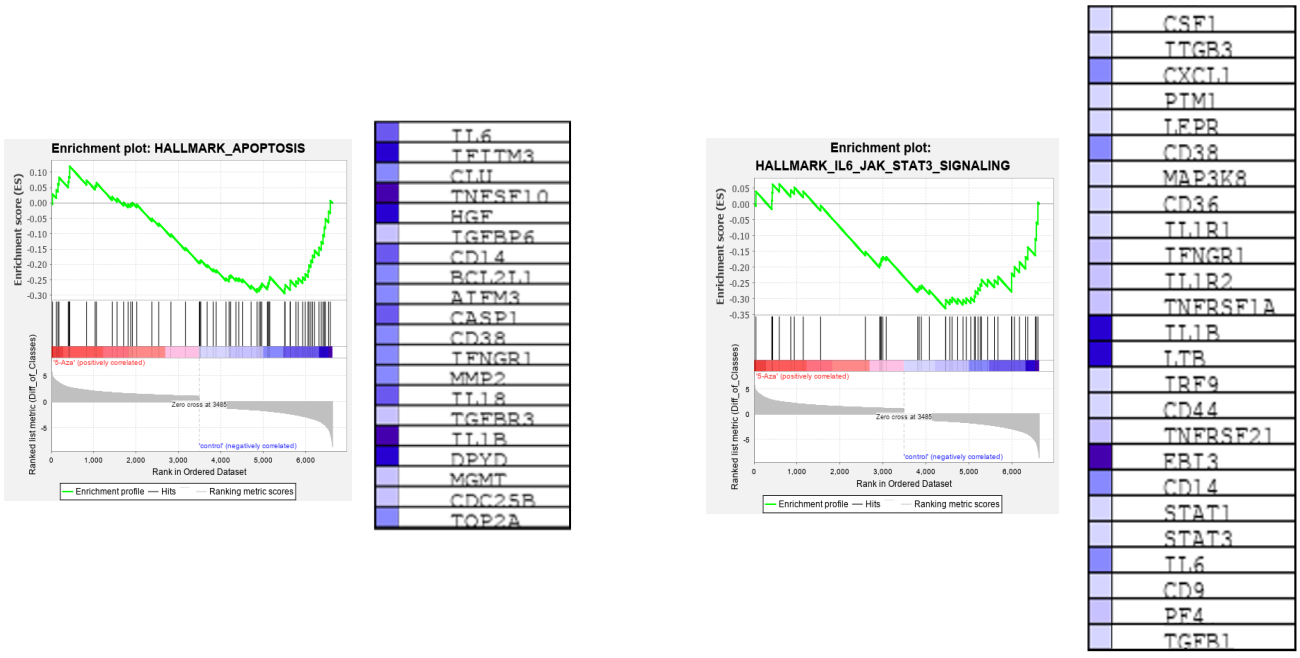

Figure 10. Set Enrichment Analysis (GSEA) of A549 Cell Line Treated with 5-Aza. The running ES indicates the degree to which this gene set is overrepresented at the top or bottom of the entire ranked list of genes. GSEA plots are a ranked list of genes from microarray analysis, sorted by their correlation with treatment effect. The color code bar (red to blue) represents the correlation of gene expression with the phenotype of interest, with red indicating a positive correlation and blue indicating a negative correlation. The leading-edge subset of genes, those contributing most to the ES, are highlighted within this list.

Downregulation of genes involved in cell cycle and proliferation

Our microarray analysis identified significant changes in gene expression in A549 cells post-5-Aza treatment. *PIM1* and *BCL3*, known for their roles in cell cycle regulation and survival, were significantly downregulated in the A549 cells following 5-Azacytidine treatment combined with 2 Gy of IR (AZA_IR) compared to the control group. *PIM1* exhibited a fold change (FC) of -3.5123045 (log FC = -1.8124179) with a corrected p-value of 1.18E-04, while *BCL3* showed a FC of -3.5693064 (log FC = -1.8356438) with a corrected p-value of 5.13E-05.

Regulation of genes in apoptosis and immune response

STAT3, a mediator in various signaling pathways, including apoptosis and immune response, was downregulated with a FC of -2.0139275 (log FC = -1.0100117, p = 8.86E-04). Conversely, *TBX21*, which plays a role in immune system activation, exhibited a significant upregulation with a FC of 55.022327 (log FC = 5.781945, p = 7.47E-05).

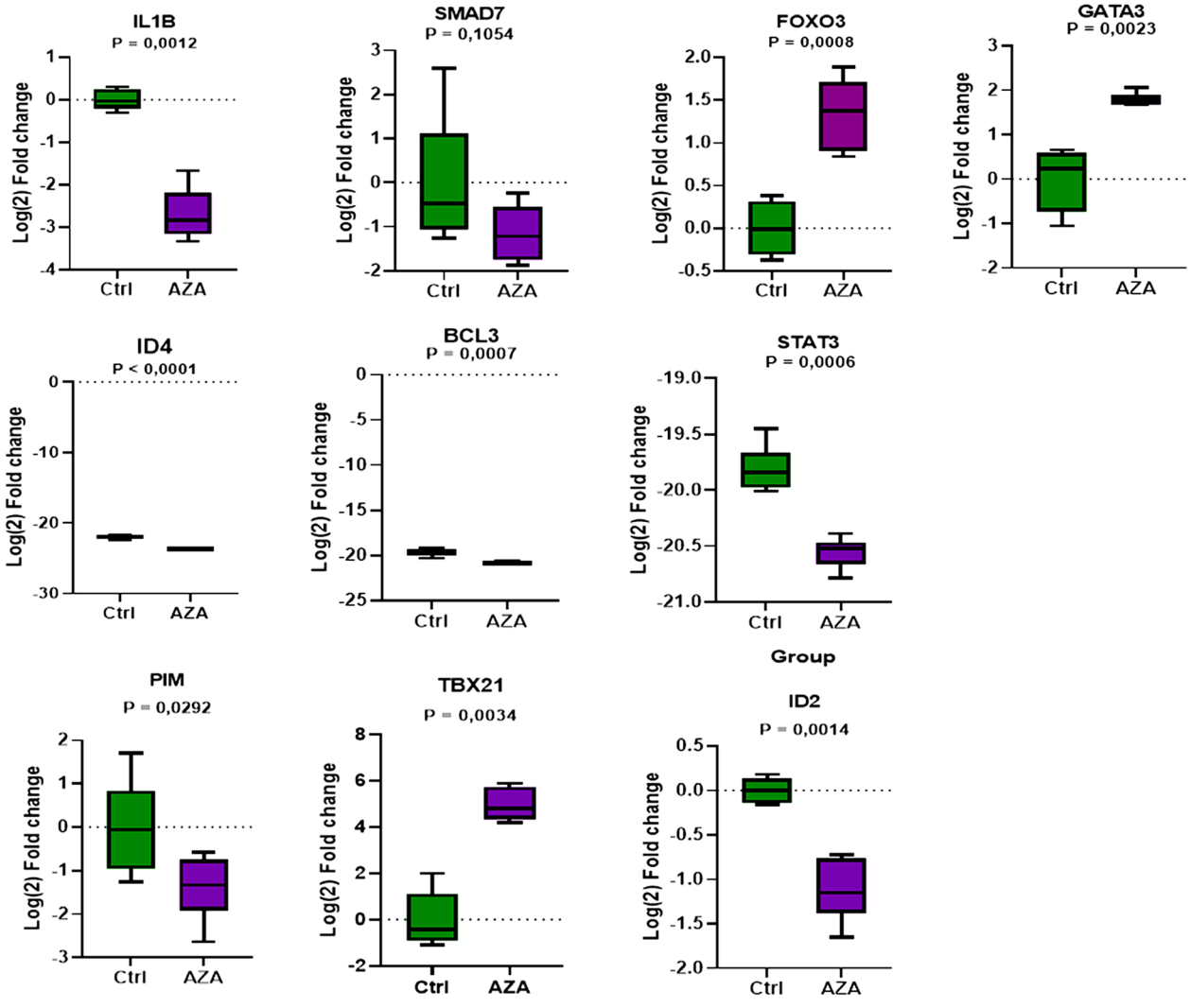

Figure 11. qPCR Validation of Gene Expression after 5-Aza treatment on A549 cell line. RT-qPCR analysis of *IL1B*, *SMAD7*, *FOXO3*, *GATA3*, *ID4, BCL3, STAT3, PIM, TBX21* and *ID2* expression in A549 Control compared A549 treated with 5-Aza - data presented as mean ± S.D.; P < 0.0012, independent t-test compared to control.

Modulation of genes involved in differentiation and inflammatory response

ID4, associated with cellular differentiation, was downregulated with a FC of -3.943673 (log FC = -1.9795399, p = 7.85E-05). IL1B, a key pro-inflammatory cytokine, also showed significant down-regulation with a FC of -36.61175 (log FC = -5.194235, p = 2.61E-06). In contrast, genes associated with T cell function and differentiation, such as *GATA3*, was upregulated with a FC of 3.2849302 (log FC = 1.7158628, p = 5.28E-04).

Changes in gene expression related to apoptosis and cell cycle regulation

SMAD7, involved in the TGF-beta signaling pathway and thus linked to apoptosis and cell cycle regulation, was downregulated with a FC of -2.0656073 (log FC = -1.046566, p = 0.001460305). *FOXO3*, a gene that contributes to cell cycle arrest and apoptosis, was upregulated with a FC of 2.7578971 (log FC = 1.4635687, p = 8.18E-04).

Influence on cell differentiation pathways

ID2, playing a role in cell differentiation, exhibited downregulation with a FC of -3.7644532 (log FC = -1.9124403, p = 5.54E-05).

Validation of microarray data through qPCR

After analyzing the transcriptional alterations in the A549 cell line post-treatment with 5-Aza, as evidenced through microarray analysis, we identified a subset of ten genes for subsequent validation. This selection was grounded on their statistically significant alterations in expression levels and their association with pathways implicated in oncogenesis. The chosen genes, namely *PIM*, *BCL3*, *TBX21*, *FOXO3*, *IL1B*, *GATA3*, *ID2*, *SMAD7*, *STAT3* and *ID4*, are integral to the regulation of various cellular processes including cell cycle control, programmed cell death, immune responses, and cytokine-mediated signaling (Figure 11).

IL1B, a pivotal mediator of inflammation, exhibited statistically significant downregulation in the Aza-treated group (P = 0.0012). SMAD7, a negative regulator in the TGF-beta pathway, also showed significant changes (P = 0.1504). *FOXO3*, involved in apoptosis and cell cycle regulation, displayed a notable increase in expression in the treated cells (P = 0.0008), suggesting an enhanced pro-apoptotic response. *GATA3*, integral to immune cell differentiation, showed increased expression with significant changes (P = 0.0023), pointing towards an immunomodulatory effect of the treatment. *BCL3*, linked with NF-κB signaling, had a marked change in expression levels (P = 0.0007), which may be indicative of altered cell survival pathways. *ID2*, a gene associated with cell differentiation, also demonstrated significant expression changes (P = 0.0014) in the 5-Aza group. Further, *PIM*, implicated in the regulation of the cell cycle and survival, showed significant downregulation (P = 0.0292). *STAT3*, an important transcription factor modulating responses to cytokines, was significantly reduced (P = 0.0006), possibly impacting cellular communication and transcriptional activation. *TBX21*, involved in the activation of the immune system, displayed an increase in expression (P = 0.0034), implying an immune response upregulation. *ID4*, as *ID2*, it is involved in cell differentiation, was observed to be significantly downregulated (P < 0.001), further supporting the differentiation inducing potential of AZA in the treatment context.

Analysis of the expression changes for selected genes, with the log (2) FC from both microarray and qPCR results, along with the corresponding p-values listed in table IV.

In vivo efficacy of 5-Aza and IR in NSCLC

Efficacy in subcutaneous xenograft model

In the subcutaneous xenograft model, A549 cells were implanted into the right flanks of mice, forming tumors that were subjected to various treatment regimens. The groups receiving treatment of 5-Aza alone or in combination with IR exhibited a significant reduction in tumor growth compared to the controls and IR only groups (Figure 12).

Table IV. Comparative analysis of gene expression changes from microarray and qPCR analysis.

Gene	Microarray log(2)FC	qPCR log(2) FC	Microarray p-value	qPCR p-value	Validation outcome
PIM1	-1.8124179	-1.38865	1.18E-04	0.0292	Both methods indicate significant downregulation.
STAT3	-1.0100117	-0.74859	8.86E-04	0.0006	Consistent downregulation reported by both methods with high statistical significance.
ID4	-1.9795399	-1.74508	7.85E-05	0.001	Downregulation is consistently observed, supported by significant p-value in qPCR.
BCL3	-1.8356438	1.21313	5.13E-05	0.0007	Microarray indicates downregulation, while qPCR suggests upregulation; both methods confirm significant changes.
IL1B	-5.194235	5.12214	2.61E-06	0.0012	Notable downregulation observed in both datasets with high statistical significance.
SMAD7	-1.046566	1.51686	0.001460305	0.1054	Microarray suggests downregulation, qPCR indicates upregulation; both are statistically significant.
FOXO3	1.4635687	-0.97961	8.18E-04	0.0008	qPCR indicates significant upregulation; microarray suggests less pronounced change.
GATA3	1.7158628	1.80431	5.28E-04	0.0023	Upregulation observed in both methods, validated by qPCR.
ID2	-1.9124403	-1.80431	5.54E-05	0.0014	Downregulation trend is consistent and statistically significant.
TBX21	5.781945	5.23369	7.47E-05	0.0034	Substantial upregulation noted in both datasets with statistical significance.

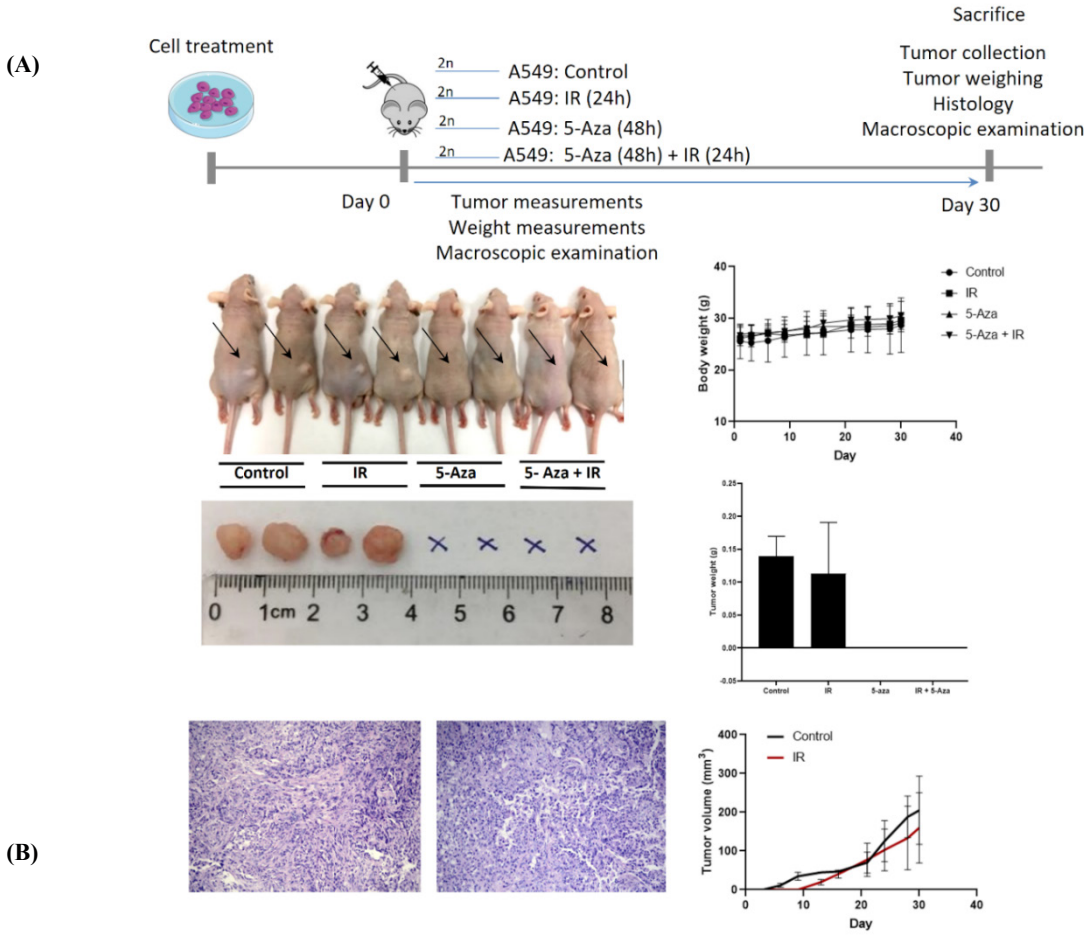

Figure 12. Evaluation of 5-Aza and IR in NSCLC Mouse Models. The timeline from panel A specifies the treatment regimen applied to the mice: Control group, IR group, 5-Aza (48 hours) group, and 5-Aza + IR (48 hours) group and the observation period. Panel B displays the experimental mice with arrows highlighting palpable subcutaneous tumors, organized into four distinct groups in accordance with the treatments administered, along body weight measuring, tumor weight, tumor volume and tumor IHC (available tumors only for control and IR).

Tumor volumes were measured and recorded over a 30 day period. The control group tumors exhibited a characteristic aggressive growth pattern, followed relatively closely by the IR group. For the case of the cells treated with either 5-Aza or 5-Aza combined with IR, no visible subcutaneous tumors were observed in the experimental timelapse, suggesting a pronounced inhibition of tumor growth (Figure 12, Panel B). The histological examination of the IR treated tissue reveals disorganized proliferation of malignant lung cancer cells, characterized by hyperchromatic and polymorphic nuclei, an increased number of mitoses, and the presence of scattered intratumoral lymphocytes, indicative of an immune response to the radiation induced cellular damage. In contrast, the control tissue would exhibit organized cell architecture and lack these signs of stress and damage.

Throughout the treatment course, body weight measurements indicated no significant changes, suggesting minimal systemic toxicity of the treatment and well tolerance.

Efficacy in orthotopic xenograft model

Orthotopic xenografts were established by injecting A549-Luc2 cells directly into the lung tissue of mice. The treatment group receiving biweekly doses of 5-Aza displayed a significant reduction in bioluminescence intensity as assessed by IVIS imaging, compared to the control group. This reduction was consistent with a decrease in the primary lung tumor burden (Figure 13).

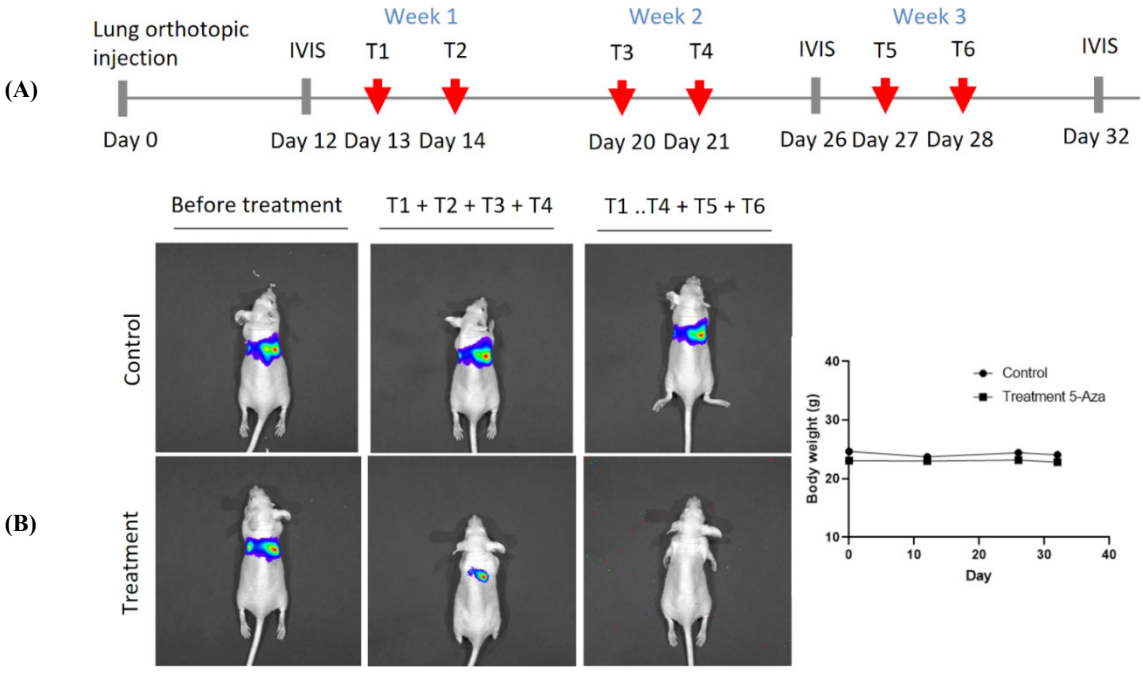

Figure 13. Bioluminescent Monitoring of Orthotopic Lung Tumors in Response to 5-Aza Treatment. A. Timetable of cell inoculation, treatment scheme and imaging timepoints. B. IVIS imaging of control mice and 5-Aza treated mice over the course of the three-week treatment, along with lung appearance after the end of the treatment and body weight measurements.

Panel A presents a timeline of the *in vivo* experiment, marking the initiation of the tumor cell injection, the commencement of treatment, and the weekly intervals at which bioluminescent imaging (BLI) was performed. Sequential BLI images are presented in Panel B, showing the progression of tumor growth in control and treated mice over 32 days. The control group shows an increase in signal intensity, reflective of aggressive tumor growth. The treatment group exhibits a diminished signal, suggesting a reduction in tumor progression due to the 5-Aza therapy, with no visible macroscopic tumors on the lungs at the end of the experiment. Also, the graphical representation of body weight changes across the treatment span, indicating the systemic impact of the treatments. The stable body weight across all groups suggests that the treatments did not induce significant toxicity that affected the overall health of the mice. This experiment highlights the potential of 5-Aza *in vivo* and supports the continuation of a similar therapeutic scheme on a larger cohort of animals for a more comprehensive validation.

Discussion

Our investigation into the synergistic effects of 5-Aza and IR on NSCLC reveals potential alternatives that can enhance the therapeutic efficiency of the current treatment schemes. 5-Aza is currently predominantly used in the hematological sector without major side effects and is considered safe for clinical administration. By evaluating both *in vitro* and *in vivo* models, this study highlights the potential of epigenetic modulation in other cancers like NSCLC, as singular therapy or in combination with traditional radiation therapy (IR).

Through a meticulous analysis of cell culture models and animal experiments, this research emphasizes the significant potential of epigenetic modifications in treating NSCLC solid tumors. We explored 5-AZA alone and in combination with IR, depicting the effect on *in vitro* and *in vivo* models, indicating that 5-AZA may induce substantial changes in the epigenetic profile of NSCLC cells, leading to gene alterations that can enhance therapy.

Our molecular examination of differential gene expression, using both microarray and PCR techniques, demonstrated that genes such as *STAT3* and *TBX21*, which are known for their regulatory functions in apoptosis and immune response respectively, exhibited changes in their expression levels. This demonstrates the ability of 5-Aza to alter the epigenetic environment, resulting in the reduction of methylation at gene promoters and the subsequent increase in the expression of these genes. Also, the study indicated that genes like *PIM1* and *BCL3* were found to be downregulated. These genes may also be associated with the hypomethylating effect of 5-Aza. However, these

changes may be more complex and include other regulatory processes apart from direct DNA methylation alterations. Regarding the functional effects, the combination of 5-Aza and IR demonstrated a synergistic role in reducing tumor cell viability, increasing apoptosis, and impairing cell migration and invasion, highlighting the enhanced therapeutic potential of the combined treatment. However, for the *in vivo* validation of the repurposed therapy we concentrated mainly on the effect of 5-Aza as demonstrated the most prominent effect upon cell behavior. Moreover, the initial *in vivo* model using subcutaneous tumor showed minimal tumor growth for both 5-Aza and 5-Aza and IR group of mice, enhancing the fact that 5-Aza is the main active therapeutic that inhibits the development of NSCLC.

The orthotopic *in vivo* models confirmed the effectiveness of the treatment, showing a decrease in both tumor size and metastasis. The findings were validated by histological and bioluminescent imaging investigations, which highlighted the promise of 5-Aza therapy in the treatment of NSCLC. These results showed that epigenetic therapy could improve treatment outcomes as single therapy or in combination with current approved treatments.

Epigenetic modifications have been mentioned in recent literature as the hallmark of hallmarks in tumorigenesis, being involved in all hallmarks of cancer. This mechanism is universal in all malignant pathologies but varies deeply between patients and cancer types. 5-Aza is a demethylating agent that counteracts the pathological profile of gene methylation without being specific for certain genes or types of cancer. For example, studies have shown that 5-Aza enhances the efficacy of radiotherapy in head and neck squamous cell carcinoma (HNSCC) and pancreatic cancer by modulating the tumor microenvironment and enhancing the immune response [19]. Therefore, in theory 5-Aza could function as a universal treatment enhancer in combination with current therapeutic schemes in oncology or as a safe alternative as singular treatment or in combination with IR for patients at high risk (e.g. advanced age) due to its safe clinical profile.

Future research should prioritize advanced preclinical and clinical trials to validate these in vitro and *in vivo* findings and optimize the dosage and treatment scheduling of 5-Aza to maximize therapeutic benefits while minimizing adverse effects. Investigating the molecular mechanisms underlying the effects of 5-Aza (and radiotherapy) could provide valuable insights into NSCLC response and also set the base for further drug repurposing strategies in additional cancer types.

Conclusions

Functionally, the synergistic interaction between 5-Aza and IR was shown to significantly lower tumor cell viability, promote apoptosis, lower cell migration and invasion capacity, indicating the potential therapeutical efficacy of this combined treatment. The *in vivo* evaluation showed limited tumor growth and decreased metastasis in the group treated with 5-AZA, while the histological evaluation and bioluminescent assay demonstrated that 5-AZA suppresses the development and progression of NSCLC. Considering the passive nature of epigenetic modifications in cancer, 5-AZA, as a demethylating agent, can reverse pathological gene methylation and presents significant potential for applications in various types of tumors.

Future research should prioritize advanced preclinical and clinical trials to validate these in vitro and *in vivo* findings and optimize the dosage and treatment scheduling of 5-Aza to maximize therapeutic benefits while minimizing adverse effects. Investigating the molecular mechanisms underlying the effects of 5-Aza (and radiotherapy) could provide valuable insights into NSCLC response and also set the base for further drug repurposing strategies in additional cancer types.

Acknowledgements

This work was supported by research grant No. PCE 185/18.02.2021 "Validation of epigenetic reprogramming of lung cancer models and anti-cancer activity through serial administration of repositioned 5-Azacytidine-AZUR", PN-III-P4-ID-PCE-2020-1957 and research grant PCD - no. 2461/48. The authors acknowledge the support from the research project — "Clinical and economic impact of personalized targeted anti-microRNA therapies in reconverting lung cancer chemo-resistance"-CANTEMIR.

References

1. Molina JR, Yang P, Cassivi SD, Schild SE, Adjei AA. Non-small cell lung cancer: epidemiology, risk factors, treatment, and survivorship. Mayo Clin Proc. 2008;83:584–594.
2. Araghi M, Mannani R, Heidarnejad Maleki A, Hamidi A, Rostami S, Safa SH, et al. Recent advances in non-small cell lung cancer targeted therapy; an update review. Cancer Cell Int. 2023;23:162.
3. Wang J, Koo KM, Wang Y, Trau M. Engineering State-of-the-Art Plasmonic Nanomaterials for SERS-Based Clinical Liquid Biopsy Applications. Adv Sci (Weinh). 2019;6:1900730.
4. Reed MD, Tellez CS, Grimes MJ, Picchi MA, Tessema M, Cheng YS, et al. Aerosolised 5-azacytidine suppresses tumour growth and reprogrammes the epigenome in an orthotopic lung cancer model. Br J Cancer. 2013;109:1775–1781.
5. Ramazi S, Daddzadi M, Sahafnejad Z, Allahverdi A. Epigenetic regulation in lung cancer. MedComm (2020). 2023;4:e401.
6. Davalos V, Esteller M. Cancer epigenetics in clinical practice. CA Cancer J Clin. 2023;73:376-424.
7. Kim DS, Kim MJ, Lee JY, Kim YZ, Kim EJ, Park JY.

Aberrant methylation of E-cadherin and H-cadherin genes in nonsmall cell lung cancer and its relation to clinicopathologic features. Cancer. 2007;110:2785–2792.

8. Belinsky SA, Nikula KJ, Palmisano WA, Michels R, Saccomanno G, Gabrielson E, et al. Aberrant methylation of p16(INK4a) is an early event in lung cancer and a potential biomarker for early diagnosis. Proc Natl Acad Sci U S A. 1998;95:11891–11896.
9. Füller M, Klein M, Schmidt E, Rohde C, Göllner S, Schulze I, et al. 5-azacytidine enhances efficacy of multiple chemotherapy drugs in AML and lung cancer with modulation of CpG methylation. Int J Oncol. 2015;46:1192–1204.
10. Cheng Y, He C, Wang M, Ma X, Mo F, Yang S, et al. Targeting epigenetic regulators for cancer therapy: mechanisms and advances in clinical trials. Signal Transduct Target Ther. 2019;4:62.
11. Tao L, Zhou Y, Luo Y, Qiu J, Xiao Y, Zou J, et al. Epigenetic regulation in cancer therapy: From mechanisms to clinical advances. MedComm – Oncology. 2024;3:e59. Doi: 10.1002/mog2.59
12. Cameron EE, Bachman KE, Myöhänen S, Herman JG, Baylin SB. Synergy of demethylation and histone deacetylase inhibition in the re-expression of genes silenced in cancer. Nat Genet. 1999;21:103–107.
13. Papageorgiou SG, Vasilatou D, Kontos CK, Foukas P, Kefala M, Ioannidou ED, et al. Treatment with 5-Azacytidine improves clinical outcome in high-risk MDS patients in the 'real life' setting: A single center observational study. Hematology. 2016;21:34–41.
14. Momparler RL. Epigenetic therapy of non-small cell lung cancer using decitabine (5-aza-2′-deoxycytidine). Front Oncol. 2013;3:188.
15. Chai G, Li L, Zhou W, Wu L, Zhao Y, Wang D, et al. HDAC inhibitors act with 5-aza-2′-deoxycytidine to inhibit cell proliferation by suppressing removal of incorporated abases in lung cancer cells. PLoS One. 2008;3:e2445.
16. Jiang W, Li YQ, Liu N, Sun Y, He QM, Jiang N, et al. 5-Azacytidine Enhances the Radiosensitivity of CNE2 and SUNE1 Cells In Vitro and In Vivo Possibly by Altering DNA Methylation. Busson P, editor. PLoS One. 2014;9:e93273.
17. De Schutter H, Kimpe M, Isebaert S, Nuyts S. A systematic assessment of radiation dose enhancement by 5-Aza-2′-deoxycytidine and histone deacetylase inhibitors in head-and-neck squamous cell carcinoma. Int J Radiat Oncol Biol Phys. 2009;73:904–912.
18. Kwon HM, Kang EJ, Kang K, Kim SD, Yang K, Yi JM. Combinatorial effects of an epigenetic inhibitor and ionizing radiation contribute to targeted elimination of pancreatic cancer stem cell. Oncotarget. 2017;8:89005–89020.
19. Xu M, Hou Y, Li N, Yu W, Chen L. Targeting histone deacetylases in head and neck squamous cell carcinoma: molecular mechanisms and therapeutic targets. J Transl Med. 2024;22:418.